Current Pathways Model for Hall Thruster Plumes in Ground-based Vacuum Test Facilities

David J. Jovel[1] and Mitchell L. R. Walker.[2]
Georgia Institute of Technology, Atlanta, GA, 30332, U.S.

Hall effect thrusters are known to perform differently in the space environment than what is measured when operated inside ground-based vacuum test facilities. The environment inside test facilities can replicate only some of the electrical boundary conditions observed in space. Specifically, most vacuum test facilities are metallic and electrically grounded, whereas the space environment possesses a low-density, cold plasma that varies in time due to space weather activity. Therefore, it is essential to understand how Hall effect thrusters electrically couple to and are affected by their local operating environment. A novel current pathways model has been developed to represent the electrical coupling between the Hall effect thruster plume and the ground-based vacuum test facility operational environment. Effective resistances, capacitances, and inductances based on the physical interfaces between the HET plume and the surrounding facility environment are derived. The current pathways model shows that charge-exchange ions resulting from elevated pressures and the electrically-conductive vacuum chamber walls assist in the overall Hall effect thruster plume neutralization process.

Nomenclature

A_{sh} = Sheath surface area, m^2

C = Capacitance, F

e = Elementary charge, 1.60218×10^{-19} C

E_e = Electron energy, eV

h = Planck's constant, 6.62607×10^{-34} Js

[1] Graduate Research Assistant, School of Aerospace Engineering, AIAA Member; david.r.jovel@gatech.edu.
[2] Professor, School of Aerospace Engineering, AIAA Fellow; mitchell.walker@ae.gatech.edu.

I_{dis} = Discharge current, A

$I_{i,beam}$ = Beam ion current, A

$I_{i,CEX}$ = Charge-exchange ion current, A

$I_{e,beam}$ = Electron current for ion beam neutralization, A

$I_{e,CEX}$ = Electron current for CEX ion neutralization, A

$I_{e,ionization}$ = Electron current for ionization, A

$I_{e,plume}$ = Electron current for plume neutralization, A

$I_{e,rec}$ = Electron current for recombination in the plume, A

$I_{e,wall}$ = Electron current to the chamber wall, A

k_b = Boltzmann constant, 1.38065×10^{-23} J/K

L = Inductance, H

m_k = Mass per particle of the k^{th} species, kg

n_k = Number density of the k^{th} species, cm^{-3}

P_{op} = Facility operational pressure, Torr

Q = Collision cross-section, m^2

R = Resistance, Ω

R_E = Earth's radius, 6378.137 km

T_e = Electron temperature, eV

V_{dis} = Discharge voltage, V

V_p = Plasma potential, V

V_s = Space plasma potential, V

V_w = Chamber wall potential, V

Z = Ion charge state

$Z_{disch,ch}$ = Effective impedance of the discharge channel, Ω

Z_{eff} = Effective ion charge state

ε_o = Permittivity of free space, 8.85419×10^{-12} F/m

λ_D = Debye length, m

ν = Electromagnetic wave frequency, Hz

ν_k = Collision frequency of the kth charge species, s^{-1}

σ_k = Electrical conductivity of the kth charge species, Ω^{-1}

I. Introduction

THE performance and stability of Hall effect thrusters (HETs) depend on their local operating environment. Ground-based vacuum test facilities used for HET performance characterization cannot replicate many aspects of the real operating environment in space. For instance, the operational pressures maintained by modern vacuum facilities today are 10^{-6} Torr and are orders of magnitude higher than the 10^{-10} Torr pressure measurements in low-Earth orbit (LEO) [1]. The difference between these two operating environments has motivated research within the electric propulsion (EP) community to characterize the impact test facilities have on the performance of thrusters. Results from these investigations have shown that the conditions inside vacuum chambers have measurable effects on thruster performance in thrust, stability, and lifetime assessments. Examples of these effects include increased erosion rates of thruster components, artificially augmented thrust measurements via the ingestion of background neutrals as propellant, and the electrical coupling of the plasma discharge to electrically-conductive chamber surfaces. These effects, formally called facility effects, can be divided into three categories: 1) contamination, 2) pressure, and 3) electrical. Of the three categories, electrical facility effects are a relatively new research area and will be the focus of this article.

Electrical facility effects studies investigate the electrical configuration of the thruster-cathode system and the resulting coupling between the emitted plasma plume and the surrounding electrically-conductive vacuum chamber. The test facility imposes a voltage boundary condition that the thruster plasma must satisfy at the chamber wall that is absent in the space environment. Thus, electrically-conductive vacuum chambers alter ion–electron recombination pathways during ground-based testing as electrons emitted from the cathode can complete the main HET discharge circuit via a current pathway through nearby chamber surfaces and effectively neutralize the ion beam without having to do so in the plume. Therefore, it is reasonable to deduce that metallic vacuum test facilities may influence the electrical I-V characteristics of HETs during performance characterization test campaigns. However, the role metallic vacuum chambers serve in accommodating HET plume ion and electron currents has not been adequately studied nor quantified for the community.

Augmenting our understanding of the electrical properties of the space plasma and vacuum test facility environments provides insight into how they may electrically interact with HET plumes and influence their dynamic

operational behavior. The SMART-1 mission in 2003 was the first to publish on-orbit data of HET operation in space and provided direct evidence that the HET discharge electrically couples to the time-varying space plasma environment [2]. The SMART-1 spacecraft measured the local space plasma potential and cathode-to-spacecraft common potential and demonstrated that both potential measurements varied with Earth's diurnal cycle, orbital altitude, and sporadic solar wind activity. Moreover, the HET flown demonstrated different oscillatory behavior in space than when tested on the ground and was shown to be related to the changing space plasma environment. Although the observations made aboard SMART-1 are of interest to the EP research community, no explanation was provided for how the space plasma environment influenced the HET discharge current oscillations. Thus, we find it prudent to quantify the relevant properties of the space plasma environment and provide a direct comparison to the operational environment maintained by modern ground-based vacuum test facilities. Of particular interest to the EP community is the plasma environment contained between the altitudes of 250 km to 36,000 km for HETs operating in LEO and geostationary orbits (GEO).

Previous work in electrical facility effects has mainly consisted of experimental studies demonstrating proof of electrical coupling between a HET plume and the facility environment. The research conducted by Walker *et al.* were the first in-depth studies to show that the HET discharge circuit electrically couples to and is manipulated by metallic conductive surfaces inside vacuum chambers [3],[4]. Multiple studies were carried out to demonstrate that both the thruster body and conductive surfaces inside the test facility provide additional current pathways during HET operation. Specifically, Walker aimed to quantify the effect of changing one of the following three variables on HET current pathways: 1) the relative position of an externally-mounted cathode with respect to the thruster centerline and chamber wall, 2) the cathode-thruster body-facility electrical configuration, and 3) the voltage of large electrodes exposed to the HET plume relative to ground. Other investigations by Peterson *et al.* unveiled that the dynamic response of HETs, in terms of peak-to-peak and root-mean-square discharge current measurements, varies based on the electrical conductivity of the thruster body and thruster body-facility electrical configuration [5]. While the cited experiments here all provide direct evidence of electrical coupling between thruster's discharge circuit with its surroundings, they do not offer a formal, theory-based structure or model to explain the observed phenomena.

The work in this manuscript provides a theoretical framework that can be used to understand the electrical coupling between HET plumes and ground-based vacuum test facility environments. To achieve this, we will examine and quantify the physical properties of pressure and the electrical conductivity of the chamber wall material and their

impact on ion and electron currents during HET operation. We will show that the elevated pressures maintained by test facilities and the electrical conductivity of their metallic walls affect the current pathways necessary to satisfy the net charge neutral boundary condition as the HET plume and the facility walls exchange charge. To transition from the framework into a current pathways model, we will use concepts from electrical circuit theory to derive equivalent resistances, capacitances, and inductances based on the physical interfaces between the HET plume and the surrounding vacuum chamber environment. As a result, the equivalent current pathways model establishes the role of charge-exchange (CEX) ions caused by elevated pressures and the conductivity of metallic vacuum chambers in the effective neutralization of the HET plume.

The organization of this manuscript is done in the following manner. In section II, we briefly review ion-electron recombination physics in plasmas to establish that the mean free path for ion beam neutralization with cathode electrons in the HET plume is greater than 6000 m. Such large mean free paths for ion-electron recombination indicate that electrically-conductive surfaces downstream of the thruster exit participate in the neutralization of the HET plume. Thus, we aim to quantify properties related to the electrical conductivity of the vacuum test facility walls and the space plasma operational environment. In section III, we show that metallic vacuum chambers allow two additional current pathways for plume neutralization when compared to space operational environment, (1) CEX ion recombination at the sides and rear facility wall surfaces with respect to the thruster exit plane and (2) beam ion recombination with downstream facility wall surfaces. In section IV, we deliver a qualitative analysis of the dominant ion and electron current pathways present during thruster operation as the baseline for the framework. Section V presents the equivalent current pathways model. In the discussion, we examine the model and show that elevated operational pressures inside test facilities and electrical conductivity of the metal chamber walls influence the plume-facility current pathways of the overall HET discharge.

II. Ion-Electron Recombination in EP Plumes

Ion-electron recombination is a well-developed theory studied in atomic physics, mainly for astrophysical and controlled nuclear fusion plasma applications. Adopting the nomenclature used in the atomic physics community, we define the ion system to be the net charge positive atom with bound electrons devoid of at least one electron. Whereas a free electron is an electron from the surrounding media that interacts with the ion system via electric body forces. For complete ion-electron recombination, the free electron must bind itself to one of the allowed energy states, called orbitals, of the ion system. In the context of EP plasmas, the ion system is the beam ion expelled from the thruster of

charge state Z, while the free electron may either be an electron sourced from the cathode or a pre-existing electron from the space or vacuum test facility environment.

There are various ion-electron recombination mechanisms; however, radiative, dielectronic, and three-body recombination are the most relevant for EP plasmas. The state relations describing the interaction between an incoming free electron with an ion system, initially in state (i), and achieving the final, electron-bound state (f) for all three processes are outlined in Eqs. (1) – (3). A brief overview of the three recombination mechanisms and their respective mean free path estimates ensues.

$$e^- + A^{Z+}(i) \rightarrow A^{(Z-1)+}(f) + h\nu \tag{1}$$

$$e^- + A^{Z+}(i) \rightarrow A^{(Z-1)+*}(d) \rightarrow A^{(Z-1)+}(f) + h\nu \tag{2}$$

$$e^- + e^- + A^{Z+}(i) \rightarrow A^{(Z-1)+}(f) + e^{-*} \tag{3}$$

A. Radiative Recombination (RR)

In radiative recombination (RR), a free electron is captured into an available energy orbital of the ion system, and its excess kinetic energy is carried away by the emission of a photon. The RR process is described by the state relationship in Eq. (1) where h is Planck's constant and ν is the frequency of the emitted photon. Fortunately, many efforts in this area have led to analytical RR cross-section models that are mainly dependent on the principal quantum number, ion charge state, and the electron temperature, T_e [6],[7]. The most used RR cross-section is Kramers' semiclassical model which works well for hydrogenic ions and low incoming electron energies. For non-hydrogenic ions, or ion systems with one or more bound electrons, Kramers' formula must be corrected for the net electric field acting during the recapture of the free electron. Zerrad and Hahn suggest using an effective charge state value, Z_{eff}, that is a function of the ion's core nuclear charge, electron temperature, and possible quantum numbers when estimating the RR cross-section [6],[7],[8]. The modified Kramers' model essentially weighs the original RR cross-section with fit parameters obtained from exact numerical results [7].

In HET plumes, we are typically concerned with the recombination of $Z = 1$ up to $Z = 3$ charge state ions with T_e's greater than 1 eV. Therefore, Z_{eff} and the modified Kramers' model are appropriate for RR cross-section estimates in HET plumes. For Xe^+, we obtain $\langle Q^M_{RR,tot} \rangle = 1.865 \times 10^{-22}$ m^2 using the modified Kramers' presented in [7]. Furthermore, if we assume a plasma density of 10^{10} cm^{-3}, we find that the corresponding mean free path for radiative

recombination for an electron temperature of 1.5 eV is greater than 500,000 m. In contrast, for cold plasmas with $T_e \approx .01$ eV, we estimate mean free paths of about 3,000 m for the same plasma density, further complementing our intuition that slower-moving electrons are more likely to be captured by the ion systems' electric field and recombine radiatively. As a result of such large mean free path estimates, RR is likely not a dominant process in the neutralization of beam ions given the electron temperatures observed in HET plumes.

B. Dielectronic Recombination (DR)

In dielectronic recombination (DR), the free electron exchanges energy with the ion system's bound electrons and temporarily excites it to an intermediate, short-lived state before achieving the final recombined state. Any excess energy is released via photon emission. DR is regarded as an indirect recombination process as it proceeds via one or more intermediate excited states, $A^{(Z-1)+*}(d)$, before recombining as described by Eq. (2). The challenge in developing analytical expressions for DR cross-sections lies in the infinite number of intermediate states that may be achieved as the free electron interacts with a multi-electron ion system. Instead, DR cross-sections are numerically obtained based on the most probable energy exchange sequences and the associated radiative decay path [9]. Detailed numerical calculations require free electron energy, radiative transition probabilities, and autoionization probabilities in going from the intermediate state to the final recombined state as inputs. The reader is encouraged to reference [10] for a thorough overview of DR theory. Our literature review yielded no published values for DR cross-sections for Xe^{+}, Xe^{2+}, Xe^{3+}, or Kr equivalent ions germane to HETs. The most relevant DR cross-section found in our review was for Xe^{8+} recombining with a free electron to form Xe^{7+} dielectronically [11]. For HET plasma plumes with electron temperature around 1.5 eV, the mean free path for DR processes ranges between 50 km to 100 km [12]. We expect this value to be smaller since the experimental values obtained in the cited work are for a smaller multi-electron ion system than the 53 or 52 electron systems present in Xe^{+} and Xe^{2+} ions.

C. Three-Body Recombination (TBR)

Three-body recombination (TBR) occurs when two free electrons interact with the ion system, one of them recombines with the ion, and its surplus energy is carried away by the second free electron, which then returns to the plasma media in an excited state, e^{-*}. This process is given in Eq. (3). TBR is considered a radiationless process as all the energy exchange occurs between the two free electrons and the bound energy levels of the ion system. Since TBR is the time-reverse process of electron impact ionization, most derivations for TBR rate coefficients use the principle

of detailed balance between ionization and recombination in equilibrium conditions. Multiple TBR rate coefficient models exist; however the model given by Hahn in [13] is most appropriate for our discussion. The mean free path for TBR processes in a HET plume with T_e = 1.5 eV and n_e=10^{10} cm^{-3} for singly-charged ions is estimated to be 6,500 m.

Based on the mean free path estimates for RR, DR, and TBR processes, it is clear that the plumes emitted by HETs remain a plasma for thousands of meters downstream of the thruster exit plane. RR is the least active mechanism when compared to DR and TBR processes. These estimates are further substantiated by experimental data where plasma probes collected ion and electron current measurements 6 meters downstream of the HET exit plane and 0.05 m away from the metallic chamber wall. If the HET plume is in physical contact with an electrically-conductive space plasma or metallic vacuum chamber walls, the conducting media downstream of the thruster exit will participate in the neutralization of the plume. Thus, we aim to understand the electrical conductivity properties of the space plasma environment and vacuum test facility walls.

III. Space and Vacuum Test Facility Environments

In this section, we enumerate the key differences between the space and vacuum test facility operational environments to show that metallic vacuum chambers allow additional current pathways related to HET plume neutralization when compared to space. First, we present an overview of the dynamic space plasma at altitudes between LEO and GEO as this is where most HETs operate. Then we discuss the vacuum test facility plasma environment and the electrical conductivity properties of metallic chambers. Finally, we compare the two environments and show how the electrically-conductive properties of vacuum chambers enable HET plume neutralization.

A. Space Plasma Operational Environment from LEO to GEO

The near-Earth space environment is considered a dynamic geophysical plasma whose properties change spatially and temporally due to space weather activity, orbit altitude, the diurnal cycle, and the terrestrial magnetic field. The altitudes in this discourse will be expressed in terms of Earth's radius, R_E, given the scale of the space environment. From about 50 km up to Earth's magnetopause at an altitude ~10R_E, there exists a diverse range of plasma regions with different species composition, T_e, and n_e [14]. The three distinct plasma regions in which EP devices frequently operate are the ionosphere, plasmasphere, and the Van Allen radiation belt and are discussed next.

The first distinct plasma environment is Earth's ionosphere which spans roughly between 50 – 1000 km. The ionosphere is a cold, moderate-density plasma consisting of ions, electrons, and neutral particles from our atmosphere, namely, N_2, O_2, O, H, He, and Ar where $n_e \approx 10^5$ cm^{-3} [14],[15]. Neutral particle collisions mainly govern transport phenomena and therefore typical electron temperatures range between 0.015 eV to 0.25 eV [15]. The ionosphere gradually transitions into the plasmasphere which extends up to about $4R_E$ along the equatorial plane. Physically, the plasmasphere forms a torus-shaped volume, composed of both ionosphere and solar wind particles, that corotates with the Earth. The plasmasphere is characterized by a lower density plasma with values around 500 cm^{-3} and slightly warmer temperatures between 0.02 eV and 0.75 eV [16]. In this region, n_e and T_e are known to decrease non-linearly density drops sharply to values less than 10 cm^{-3} [17]. The Van Allen radiation belt region blends in between the plasmapause and the magnetopause where highly energetic electrons and protons, mainly from the solar wind, are magnetically confined. The radiation belt contains a low-density plasma in the 10^{-1} cm^{-3} range but much more energetic particles with $T_e > 1$ keV [18]. EP devices used aboard GEO satellite platforms straddle between the outer edge of the plasmasphere and the Van Allen radiation belt are exposed to this plasma environment during operation. Garrett characterizes the plasma environment at GEO using data collected on three flight programs over a period of two years in [19]. Average plasma parameters based on this data show that $n_e \approx 1$ cm^{-3} and $T_e \approx 2.3$ keV.

Pressure in the space operational environment is proportional to number density of the local composition and can be 10^{-10} Torr or less. For LEO mission altitudes between 500 – 600 km, the pressure has been measured to be around 10^{-10} Torr [1]. Above this altitude, pressure steadily decreases based on the variation of number density through the three plasma regions as discussed previously. Once at GEO, the pressure is expected to be less than 10^{-12} Torr [20].

The physical characteristics of the three plasma regions examined confirm that space is a low-density, cold plasma operational environment that varies spatially and in time. The electron number density generally decreases precipitously as the altitude increases whereas the electron temperature reveals the opposite trend. Since the electrical conductivity of plasmas is proportional to n_e, and n_e is largest in the ionosphere, we estimate the electrical conductivity to be $10^2\,\Omega^{-1}\text{m}^{-1}$ for the space operational environment [21]. Moreover, the variation of n_e and T_e as a function of time and altitude implies that the local space plasma potential, V_s, varies accordingly. Evidence of this variation was captured aboard the SMART-1 mission in 2003 where V_s fluctuated between 16 V and 25 V with a periodicity of about 24 hours as the spacecraft ascended in orbital altitude from 1.3 R_E to 7.5 R_E during a GEO transfer orbit raising maneuver.

B. Vacuum Test Facility Operational Environment and Metallic Chamber Properties

Prior to integrating an EP device on a satellite and operating it in space, the thruster's performance is characterized inside ground-based vacuum test facilities. Vacuum test facilities are large cylindrical enclosures, typically made from metal, that utilize specialized pumps to remove air and the propellant exhausted from EP devices and simulate the low-pressure environment observed in space. Vacuum chambers range in size with diameters and axial lengths smaller than 6 m and 20 m, respectively, and much smaller than the mean free path of ion-electron recombination in the plume [22]. We briefly review the electrical conductivity properties of metallic vacuum facilities and the operational pressures they achieve.

The metal chamber wall is an electrically-conductive medium that is typically fixed at ground potential. The type of metals used are primarily aluminum alloys or austenitic stainless steels. We can estimate the number density of free conduction electrons in these metals at room temperature based on their respective Fermi energy levels. For aluminum and 304 stainless steel, the electron number densities are 18.1×10^{22} cm^{-3} and 17×10^{22} cm^{-3} at room temperature, respectively [23]. The electrical conductivity of these metals is a function of temperature which can vary between 14 K on cryogenic pumping surfaces and above 600 K for some of the plasma-exposed surfaces. For 304 stainless steel, we can expect electrical conductivities on the order of 1.3×10^{6} $\Omega^{-1}m^{-1}$ [24]. Moreover, the electrons are in thermal equilibrium with the chamber wall and thus T_e is approximately 300 K or 0.026 eV.

The operational pressures maintained inside vacuum chambers are limited by the state of the art in vacuum pump technology and the mass flow rate into the facility. Typically, facility designers aim to maintain an operating pressure around 10^{-6} Torr for moderate thruster mass flow rates in the 10's of mg/s [25]. At these pressures, the background medium inside the chamber is considered transitional flow with neutral number densities > 10^{11} cm^{-3}. In addition, the chemical composition of the vacuum chamber environment is a mixture of air constituents, residual propellant, and outgassed matter from protective structures that reside inside the facility. For example, graphite is typically used inside test facilities to shield critical diagnostics or sensitive chamber surfaces from the thruster plume due to their low sputtering yield [26],[27].

C. Comparison of the Space and Vacuum Test Facility Operational Environments

We compare n_e, T_e, and pressure of the space plasma and the ground-based vacuum facility environment. We show that the vacuum chamber provides two additional current pathways during HET operation in comparison to the space

environment. The first current pathway is via the electrically-conductive facility surfaces as HET beam ions recombine with free electrons inside the metallic wall. The second current pathway is associated with CEX ion currents that diffuse radially outward from the plume and toward chamber surfaces and attributed to elevated facility pressures. The two additional current pathways are discussed next.

The first pathway is derived from the physical interaction of the HET plume with the n_e and T_e profiles observed in space and inside metallic vacuum test facilities. In space, the electrically-conductive HET plume is allowed to freely expand indefinitely into the space plasma environment and engage with local charge species in recombination processes. The space operational environment between LEO and GEO is a low-density plasma characterized by $1< n_e <10^5$ cm^{-3} and $0.01 < T_e < 3$ keV. Referencing the ion-electron recombination models reviewed in section II, the low n_e's and moderate T_e's observed in space indicates that the mean free path for HET plume ions recombining with the low-density plasma electrons is much greater than 10^6 m. As such, neutralization of HET plumes with the local space plasma is unlikely and ion-electron recombination is predominantly achieved via cathode electrons. In contrast, during ground-based testing HET plume expansion is limited to about 10 m before it comes into physical contact with vacuum test facility walls downstream. These metallic vacuum chambers are electrically conductive with n_e's on the order of 10^{22} cm^{-3} and T_e's less than 0.03 eV. The mean free path for HET beam ions to recombine with chamber wall electrons is estimated to be less than 2 μm assuming a TBR process. Therefore, HET plume neutralization with the metallic test facilities walls is more likely than with cathode electrons. Consequently, vacuum chambers provide an additional current pathway associated with HET plume neutralization through its electrically-conductive body that is not present in space.

The second pathway is related to the elevated pressures observed inside vacuum test facilities. The operational pressure inside vacuum chambers is 1000 times greater than the LEO environment and more than 10^6 times greater than the pressures at GEO. The elevated pressures inside vacuum chambers produce higher concentrations of CEX ions, that are a non-negligible segment of the overall charged species population, with collision frequencies around 5 kHz for 300 eV xenon ions [28]. CEX ions are distinct from HET beam ions in that they are slow, with thermal velocities less than 2% of the accelerated beam ions, and roughly isotropic moving in all directions. Thus, a portion of the main ion beam current is converted into CEX ion currents that flux radially outward from the plume and are prevalent all throughout the facility. CEX ions must also recombine with electrons to maintain a quasi-neutral plasma.

The mean free path for CEX ion–electron recombination is also greater than 6000 m since recombination is governed by the same n_e's and T_e's observed in HET plumes. As a result, CEX ions also neutralize at facility surfaces.

Figure 1 presents a schematic of the current pathways. Figure 1a) depicts a cross-sectional view of the HET's discharge channel, discharge power supply, cathode, and related electron pathways for ionization and neutralization. The simplicity of the schematic aims to orient the reader with respect to ion and electron current pathways in the space environment without a space plasma. In both the space and vacuum facility operational environments, the cathode supplies electrons for propellant ionization. The difference in the electrical properties of the two environments yields differences in the electron current pathways necessary to satisfy the charge neutral boundary condition downstream. In space, the cathode electron current into the plume is the primary current pathway for ion beam neutralization and is illustrated in Figure 1a). In contrast, ground-based test facilities provide two additional current pathways that affect and participate in the overall neutralization of the HET plume: 1) the electrically-conductive facility walls and 2) elevated facility pressures. In the vacuum facility, the beam ions travel a short distance downstream of the thruster exit and recombine with free conduction electrons inside the metallic wall. In parallel, elevated pressures divert some of the anisotropic ion beam current into CEX ion currents that are slower and ubiquitous throughout the facility enclosure. Since the two distinct ion populations are neutralized with chamber wall electrons, the cathode provides a net electron current to the facility walls to satisfy a charge neutral plume-facility interface. Figure 1b) depicts the two additional current pathways allowed inside vacuum chambers during HET operation. Based on the differences in current pathways between the two operational environments, we aim to develop a model that represents how the plumes emitted by HETs electrically couple to metallic vacuum chambers during ground-based testing.

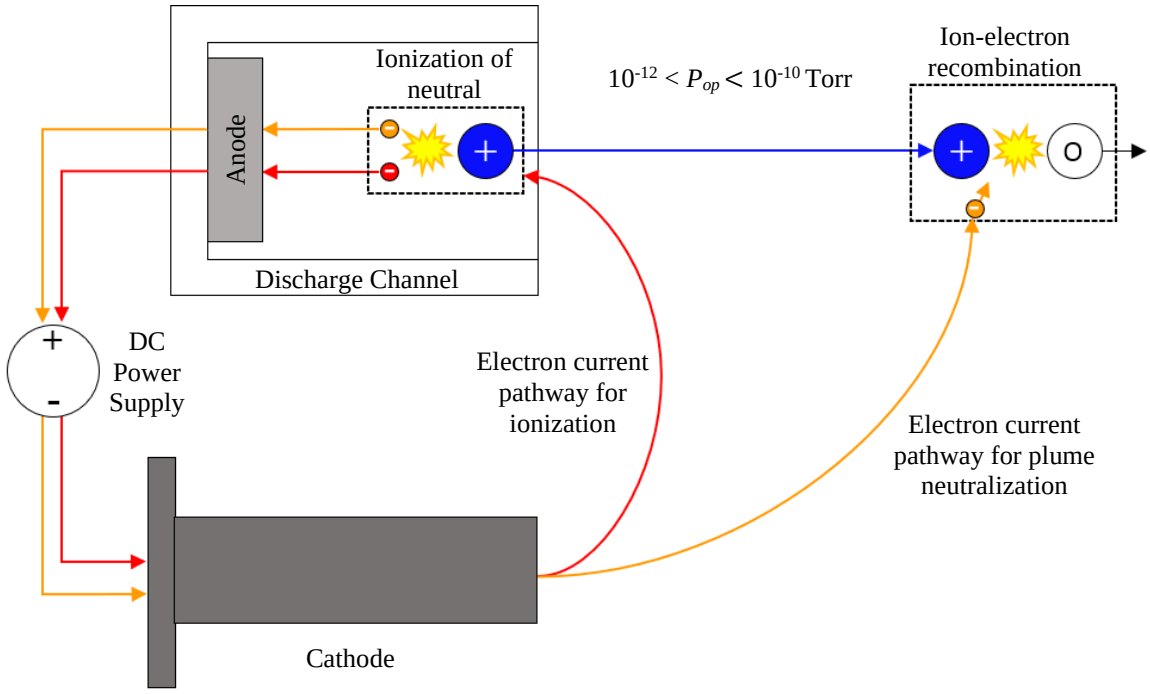

a)

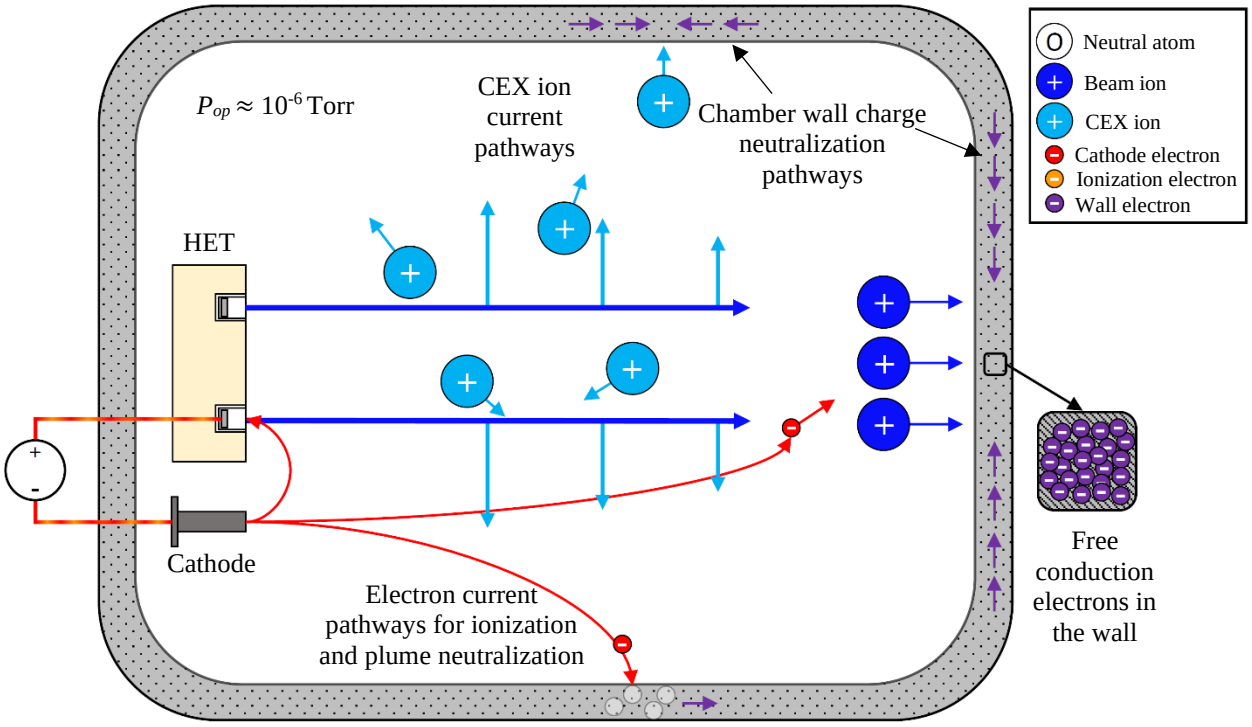

b)

Figure 1. Ion and electron current pathways related to HET plume neutralization in a) space and b) ground-based vacuum test facilities

IV. HET Ion and Electron Current Pathways inside Vacuum Test Facilities

In this section, we focus on the operation of HETs inside ground-based vacuum test facilities. We will formalize the qualitative HET currents discussion from the previous section into tractable current pathways to develop a model. In this pursuit, Figure 2 depicts a map of the various ion and electron current pathways present as a HET is operated inside a vacuum chamber. The arrow on each pathway denotes the direction of travel of the charge species and dashed circles represent charge sources or sink sites, ionization and recombination, respectively. We note that there are infinite current pathways, each transporting different rates of charge, occurring all throughout the facility at the same time. For simplicity, we have reduced the three-dimensional (3D) plasma environment to the dominant pathways shown in Figure 2 to help streamline our discussion.

In Figure 2, the control volume for our examination encapsulates the HET plume and background facility environment but does not include the HET discharge channel. The cathode emits sufficient electrons to achieve propellant ionization inside the thruster's discharge channel ($I_{e,ionization}$) and ion beam neutralization downstream into the plume. We begin at the ionization zone (1) where ions are produced and expelled downstream of the exit plane forming the ion beam current ($I_{i,beam}$) shown in blue. Depending on the facility operational pressure, some of the beam ions may undergo charge-exchange collisions with background neutral particles, roughly in thermal equilibrium with the chamber wall, to produce slow-moving CEX ions. The CEX collisions occur at (2) with the newly generated CEX ion current ($I_{i,CEX}$) shown as teal blue in Figure 2. The fraction of beam ions that do not engage in CEX can either neutralize via ion-electron recombination events within the plume (3) or continue to move downstream until they reach the chamber wall. Once at the chamber wall, the beam ion may neutralize by recombining with one of the free conduction electrons offered by the metal surface (4). The CEX ion population may also neutralize in the same manner as depicted by (5) and (6).

The cathode supplies an electron current for each of the recombination sites to maintain a net charge neutral HET plume and facility. The three cathode electron current pathways are $I_{e,CEX}$, $I_{e,beam}$, and $I_{e,wall}$ as shown in red in Figure 2. However, we quantified the mean free path of ion-electron recombination in the plume for typical n_e's and T_e's observed in EP devices to be much greater than the length scales observed inside vacuum test facilities. Therefore, the electron current pathways representing cathode electrons recombining with CEX or beam ions are small in magnitude and plume neutralization occurs predominantly through the metallic chamber wall. Consequently, $I_{e,wall}$ represents the

cathode electron current to the chamber wall necessary to replenish the metal body as its free conduction electrons are used to neutralize ion populations elsewhere in the facility (7).

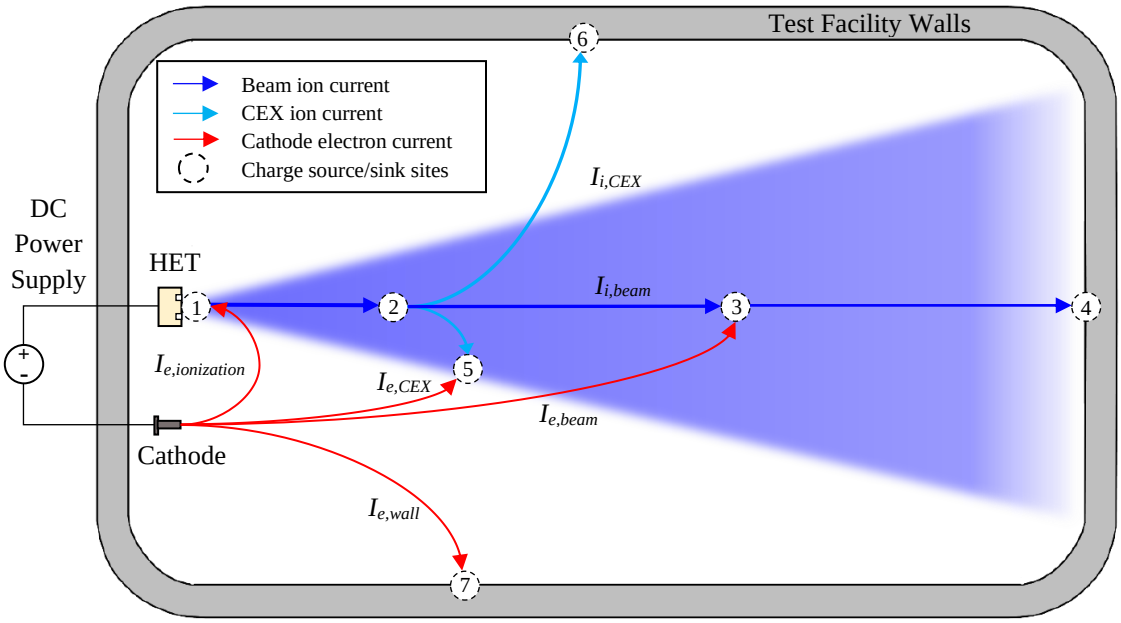

Figure 2. Schematic of ion and electron current pathways inside a vacuum test facility

A. Proposed Framework for an Equivalent Current Pathways Model

Our goal is to organize the current pathways mapped in Figure 2 using concepts and elements from electrical circuit theory so that it can be analyzed to quantify and understand the role metallic vacuum chambers play on the overall HET discharge circuit. Our proposed framework to develop a representative HET discharge-facility current pathways model is as follows. The 3D, non-uniform plasma encapsulated by the vacuum facility will be reduced to effective current branches and node locations that can vary in time, for a given thruster-cathode-facility electrical configuration. We will track both positive and negative charge species throughout the model to serve as a visual map of the distinct ion and electron current pathways inherent to the vacuum test facility environment. The various current pathways discussed previously will be organized into circuit branches with resistors, capacitors, and inductors to capture their physical processes. The five dominant processes occurring simultaneously and throughout the facility during HET operation are: 1) beam ions colliding with background neutrals producing CEX ions at elevated pressures, 2) beam ion-electron and CEX ion-electron recombination events within the plume, 3) beam ions fluxing to the facility

walls and recombining with chamber wall electrons, 4) CEX ions fluxing to the facility walls and recombining with chamber wall electrons, and 5) cathode electrons fluxing to the facility wall to replenish the deficit of facility wall electrons that recombine with ions elsewhere. These spatiotemporal microscopic processes are represented as bulk, macroscopic processes that occur at effective electrical nodes. The model is closed by imposing a net charge neutral boundary condition between all the ion and electron pathways mapped as the HET plume couples to the metallic facility walls.

Additionally, we will divide the 3D plasma environment within the facility into two distinct regions. The first region is the high-energy HET plume plasma consisting of beam ions and cathode electrons contained within a cone with a half-angle equal to the measured beam divergence half-angle. The second region is the plasma outside of the HET plume, what we will call "background plasma", consisting of only CEX ions and cathode electrons. The two regions have unique plasma properties characterized by effective T_e, n_e, and V_p's. Dividing the plasma environment in this manner allows us to map the current pathways for the two distinct ion populations as they interact with the facility and further reducing them to parallel current branches each with different properties.

Complex impedances throughout the model are assigned based on the physical processes governing how the two plasma regions interact with the facility walls. From fundamental plasma physics, we know that a plasma sheath must form to merge the electric potential boundary conditions between the local plasma and a solid surface. Two effective plasma sheaths are used to describe the interface between the plume-facility wall and background plasma-facility wall. The plasma sheath is treated as having a capacitance and resistance in parallel as derived by Chen in [29]. From Ampere's Law, we know that the ion beam will generate an azimuthal magnetic field as it expands downstream. The strength of the generated magnetic field is proportional to the enclosed ion beam current and can magnetize electrons in the plume exhibiting self-inductance. This process is regarded as an inductor and resistance in series [30].

Resistances throughout the model are derived from the inverse of the conductivity of the plasma at their respective locations. The plasma conductivity for each charge species is determined from momentum conservation equations and relevant collisional events in one dimension. Since the electrons are highly mobile, their momentum scattering cross-sections and sensitivity to small E-field perturbations are important for estimating conductivity in 1D. The relevant collisions for electrons are electron-ion elastic, electron-electron elastic, electron-neutral elastic, and electron-neutral inelastic and are denoted as $\nu_{e,tot}$. An effective inductance term can be extracted from the electron's momentum equation that represents their delayed inertial response due to a small fluctuation in the local E-field of frequency ω.

The ions are 10^6 orders of magnitude heavier than electrons and therefore mainly exhibit momentum loss due to ion-neutral CEX collisional events, ν_{io}^{CEX}. The conductivities for both electrons and ions are presented in Eq. (4) and Eq. (5), respectively [30].

$$\sigma_e(\omega) = \frac{e^2 n_e}{m_e\left(\nu_{e,tot} + j\omega\right)} \tag{4}$$

$$\sigma_i = \frac{e^2 n_i}{m_i \nu_{io}^{CEX}} \tag{5}$$

To close the pathways model, we represent an independent electron current that fluxes to the wall with its own effective sheath. This current pathway is modeled as an effectively lower resistance pathway between the cathode and nearby, electrically-conductive chamber surfaces. The cathode electrons then conduct through the chamber wall medium and replenish the net deficit of wall electrons from beam and CEX ion recombination events thereby maintaining a net charge neutral test facility.

The anode-cathode current pathway into the thruster discharge channel is regarded as a complex impedance element. The discharge channel region hosts ionization, acceleration, and various non-uniform, time-dependent azimuthal processes. We assume that the complex impedance for the discharge channel processes is the same in both the space and vacuum chamber operational environments. Therefore, the effective impedance representing ionization, acceleration, and E×B drift processes inside the discharge channel remains constant and outside the focus of this model.

Lastly, the assumptions we will make in developing an equivalent current pathways model are explicitly outlined next. First, we assume that the cathode is the only electron source in this model, and secondary electron emissions from chamber surfaces are neglected. Second, the plasma environment inside the test facility is a cold plasma, consisting of singly-charged ions, propellant neutrals, and Maxwellian electrons. Residual atmospheric constituents or sputtered materials are ignored. Third, we assume that the 3D electromagnetic phenomena occurring throughout the facility can be spatially confined to discrete *R*, *L*, and *C* electrical components at effective node locations. In doing so, we can represent the thruster plume-facility coupling as an electrical load with a complex impedance. Lastly, no net charge is allowed to accumulate on any of the components in the circuit. This assumption guarantees that the HET plume – facility current pathways segment remains net charge neutral.

V. HET Plume-Facility Current Pathways Model

We have developed an equivalent current pathways model that captures the electrical coupling between the HET plume and ground-based vacuum test facility. Figure 3 shows the model, and only one cross section of the HET's discharge channel is depicted for clarity. The model will be used to understand how plume-facility interfaces can potentially influence the effective impedance of the overall HET discharge.

The HET discharge circuit is fragmented into discharge channel processes and HET plume-facility processes as indicated by the two dashed boxes in Figure 3. The DC power supply is connected to the anode and cathode electrodes, as shown, and is the only energy source for the circuit. The "Discharge Channel" branch of the model conducts the full discharge current, I_{dis}, at the fixed discharge voltage, V_{dis}. We establish that I_{dis} is a time-varying parameter and is regarded as an AC current with a mean DC value defined by the nominal discharge operating point of the thruster. The "HET Plume - Facility" segment encompasses all the ion and electron current pathways required to satisfy plume neutralization and is the focus of this model. The positive current flow convention is adopted to remain consistent with circuit theory in electrical engineering. For locations at which ion-electron recombination events occur, we use dashed circles with 'R' throughout the circuit, indicating a current sink. At the same time, neutral-electron ionization inside the thruster discharge channel is denoted with 'I' and represents a charge source. The two current segments are discussed separately with an emphasis on the HET Plume-Facility current pathways.

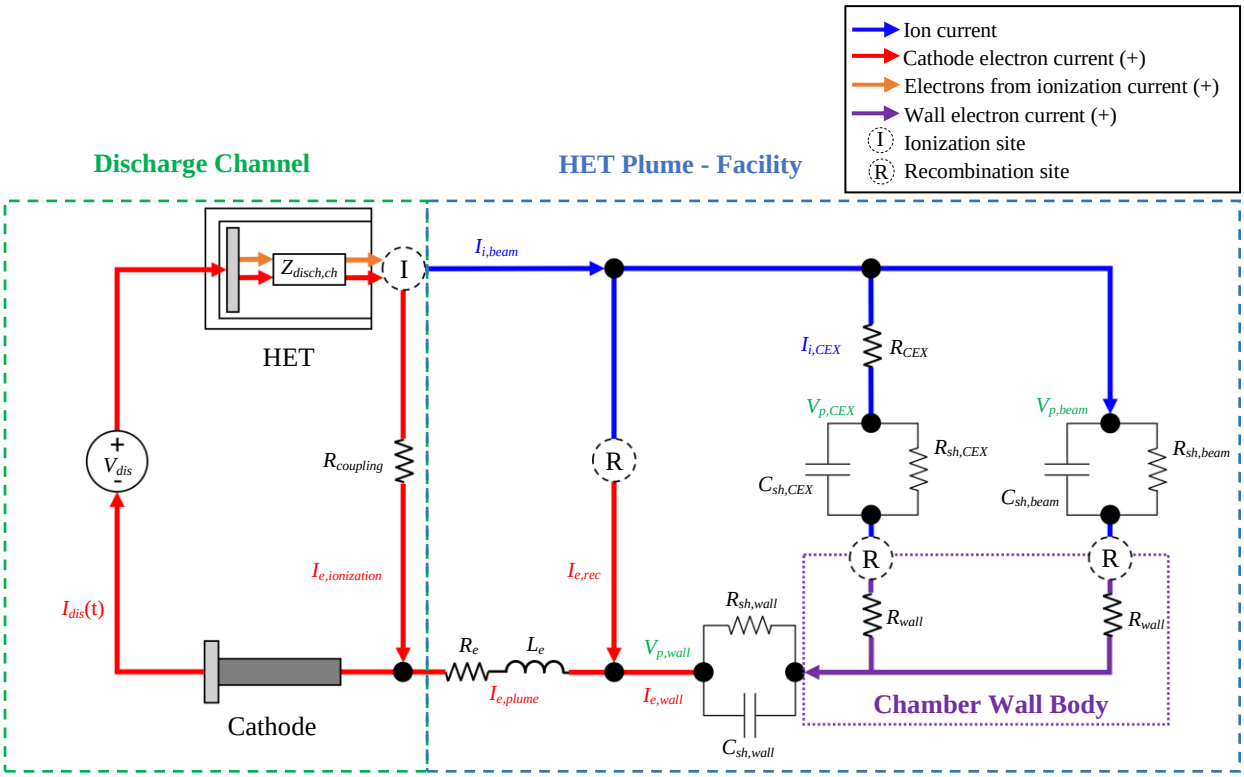

Figure 3. HET Discharge-Facility Current Pathways Model

A. Discharge Channel Current Pathway

The total electron current emitted by the cathode, I_{dis}, is the summation of the electron current for ionization, $I_{e,ionization}$, and the electron current for charge neutralization in the plume, $I_{e,plume}$. As the electrons conduct from the cathode orifice to the discharge channel, they encounter collisions with local neutrals, ions, and other electrons. Stray magnetic fields from the thruster further influence the trajectory of electrons in this region. The energy dissipated in this coupling pathway is assumed to be purely resistive and defined to be $R_{coupling}$. Once the cathode electrons arrive at the thruster exit plane, they are magnetized and endure high-energy collisions with incoming neutral atoms producing ions at the node 'I' in Figure 3. The products of an idealized $Z = 1$ ionization event are an ion and two electrons. One of the electrons is the colliding cathode electron, often called the primary electron, and the second electron is the electron stripped away from the atom after the ionization event. The electron current generated from these ionization events is colored orange in Figure 3. In addition to ionization, electrons inside the discharge channel experience E×B drift and other non-uniform, time-dependent azimuthal processes [31]. The complex processes occurring inside the thruster's discharge channel are given by the impedance $Z_{disch,ch}$. We assume that $Z_{disch,ch}$ is a weak

function of the operational environment because the processes contained therein are mainly dictated by user-defined operational parameters set by electromagnetic coil currents, anode and cathode mass flow rates, and V_{dis}. Therefore, $Z_{disch,ch}$ will be regarded as a constant and outside the focus of this model.

B. HET Plume-Facility Current Pathways

The current pathways to the right of the Discharge Channel branch all comprise the thruster plume neutralization pathways inside ground-based vacuum chambers. The ion beam current originating in the discharge channel, $I_{i,beam}$, is depicted in blue and runs along the topside of the circuit whereas the electron current for plume neutralization, $I_{e,plume}$, is shown in red at the bottom. We can decompose $I_{e,plume}$ into $I_{e,rec}$ and $I_{e,wall}$ which are the necessary cathode electron currents to neutralize both beam and CEX ions everywhere in the facility. The electron inductance due to oscillations, Beam-CEX ion resistance, and plasma sheath capacitance are discussed in the subsequent sections.

1. Effective Inductance of Electrons in an Oscillating Plume

An oscillating E-field of a certain frequency will cause the electron conductivity to vary at the same frequency exhibiting an effective inductance. The electron conductivity provided in Eq. 4 can be separated into a real component that is a function of $\nu_{e,tot}$ only and an imaginary component that is a function of the oscillating frequency, ω. Comparing the definition of inductive reactance to the imaginary term in the electron conductivity yields an effective inductance, L_e, that is a function of n_e and plume-facility geometry lengths l_{eff} and A_{eff} as given in Eq. (6) below.

$$L_e = \frac{m_e l_{eff}}{e^2 n_e A_{eff}} \tag{6}$$

Selection of the geometric parameters l_{eff} and A_{eff} is dependent on facility geometry relative to the cathode orifice. We assume that the electron medium fluxes perpendicular to the planar cross-sectional area of the test facility and that l_{eff} is given by the axial length of the chamber. Typical values for L_e are small and around 1.5 nH for 10^{10} cm^{-3} and becomes a more pronounced reactance at oscillating frequencies greater than 1 MHz.

2. Beam-CEX Ion Resistance

The third pathway represents the generation and neutralization of CEX ions due to elevated facility pressures. In Figure 3, a fraction of the ion beam current is diverted to CEX ion current via collisional events. Since we are tracking

the momentum of charged particles throughout the model, a 300-eV beam ion exchanging charge with a slow-moving neutral atom appears to have lost much of its initial momentum in one direction. We represent this momentum loss by R_{CEX} and is provided by Eq. (7). For convenience, we have expressed R_{CEX} in terms of measurable inputs such as facility operational pressure, P_{op}, chamber wall temperature, T_w, mean CEX collision rate coefficient, $\langle \mathrm{v}_i Q_{CEX} \rangle$, and plume-facility geometry lengths l_{eff} and A_{eff}.

$$R_{CEX} = \frac{m_i P_{op} \langle \mathrm{v}_i Q_{CEX} \rangle l_{eff}}{e^2 n_i k_b T_w A_{eff}} \tag{7}$$

For this resistance, the choice for l_{eff} and A_{eff} are based on an effective location within the ion beam divergence cone at which CEX is assumed to occur. For example, l_{eff} can be the axial length between the thruster exit plane and the downstream facility wall, while A_{eff} can be the area of a circular cross-section of the expanding ion beam at $l_{eff}/2$. Consider a HET accelerating 300-eV xenon ions with a beam divergence half-angle of 25° and $P_{op} = 1\times10^{-5}$ Torr-Xe, $T_w = 300$ K, $n_i = 10^{16}$ m^{-3}. Moreover, we reference [28] to obtain $Q_{CEX} = 5.4\times10^{-19}$ m^2 for 300 eV xenon ions. If the expanding ion beam has an axial length of 6 m, then the R_{CEX} is estimated to be 3 Ω.

3. Plasma Sheath Capacitance at the Walls

The CEX ion population constituting the background plasma fluxes radially outward of the HET plume region to the chamber wall. The remaining ion beam current continues uninhibited to the facility wall directly downstream of the HET exit plane. A plasma sheath forms between the two distinct plasma regions and the facility wall. We use the sheath capacitance from Chen in [29] to model the electrical interface between the two plasma regions and the metallic chamber wall. For completeness, the sheath capacitance, C_{sh}, appropriated from Chen, is provided below in Eq. (8). The sheath resistance, R_{sh}, is governed by the conductivity of electrons fluxing through a 10 Debye length thick sheath and given by Eq. (9).

$$C_{sh} = \frac{A_{sh}}{2.38}\left(\frac{\varepsilon_o n_e e}{T_e}\right)^{1/2}\left(\frac{(V_p - V_w)}{T_e}\right)^{-0.75} \tag{8}$$

$$R_{sh} = \frac{m_e \nu_{e,tot} 10\lambda_D}{e^2 n_e A_{sh}} \tag{9}$$

It is clear from Eqs. (8) and (9) that to estimate the capacitance and resistance of the plasma sheath, the local plasma properties are required. Data collected in previous test campaigns by this author have given us insight into the plasma properties for the background plasma and the plume plasma regions. The physical boundary distinguishing the two plasma regions is provided by the intersection of the diverging ion beam with the facility wall enclosure. The sheath area, A_{sh}, is the wetted facility surface area incident to the plasma region of interest. The sheath capacitance for both plasma regions is on the order of μF, and the sheath resistance is negligible and below 5 μΩ.

VI. Discussion

The model shows that the high electrical conductivity of the metal chamber walls assists in the neutralization of the two additional current pathways observed inside ground-based test facilities. The first neutralization pathway of the HET Plume-Facility model segment in Figure 3 represents the recombination of cathode electrons with either beam or CEX ions. As established in section III, the recombination of ions with cathode electrons with T_e's of about 1.5 eV requires thousands of meters and instead will favor recombination with the metal chamber wall's free electrons. Since recombination in the plume is unlikely, we can regard the first neutralization pathway in the model as having a much higher effective resistance compared to the electrical conductivity of the chamber wall body. Thus, the model appropriately captures that the dominant neutralization pathway for both ion current populations occurs through the metal chamber walls. Furthermore, the rate at which test facilities electrons recombine with HET ion current pathways is proportional to the electrical conductivity of the wall material. Regardless, we find it constructive to keep the plume ion-electron recombination current pathway in the model as it is the dominant pathway in the operational space environment given the low-density plasmas observed there, as described in section III. Additionally, as more work is done in understanding and modeling ion-electron recombination mechanisms pertinent to EP plasmas, this neutralization pathway can be better quantified and a measurable input to the overall HET discharge impedance characteristics.

The model also reveals a direct link between the current pathways related to ionization inside the discharge channel and the pathways related to neutralization in the plume. Imposing the net charge neutral boundary condition across the HET plume-facility segment requires that the sum of all the charge sinks at the recombination sites be exactly balanced by the charge source due to ionization. Thus, if the ionization rate inside the HET is fixed and mainly governed by the user-defined operating parameters, then plume neutralization processes downstream are also influenced by the same operating parameters. The dependency of plume neutralization on $I_{i,beam}$, $R_{coupling}$, $Z_{disch,ch}$

upstream and the conductivity of the test facility walls downstream is more likely a stability concern for high-power HETs since the quantity of both beam and CEX ion current populations fluxing to the walls increase.

The capacitance of the plasma-wall sheath is the main complex impedance element in the HET Plume-Facility pathways segment with reactances that effectively alter ion and electron current fluxes to the chamber wall. The model shows that the sheath capacitors for the background plasma, plume plasma, and electron-wall plasma regions all interact to satisfy the net charge neutral condition. If certain current pathways are more prevalent than others throughout the facility, the associated plasma-wall capacitor can influence the remaining current pathways. For instance, as the facility pressure increases, so will the sheath capacitance for the background plasma region. As a result, ion-electron current pathway fluctuations may be attenuated and absorbed by the background plasma sheath capacitor, potentially concealing related I_{dis} instabilities.

Finally, converting the current pathways model into an equivalent HET discharge-facility electrical circuit has many limitations. There are three main challenges we must address in this transition. The first main challenge is that the plasma environment inside vacuum chambers is 3D and inhomogeneous, with discernible plasma properties inside and outside the emitted thruster plume. The ion beam is characterized by an ion velocity distribution function in energy and direction as well as volumetric expansion downstream. Additionally, there is a slower-moving CEX ion population emanating from the plume that randomly fluxes to all parts the facility and exhibits different plasma properties than the highly energetic plume plasma. Furthermore, the 3D shape of the vacuum chamber with respect to the location of the thruster results in varying distances and therefore the chamber wall shares its conduction electrons for recombination events at different rates depending on the local influx of ions. In contrast, electrical circuits require that electromagnetic phenomena be spatially confined to discrete bodies like resistors, capacitors, and inductors. A second impediment is that the plasma consists of multiple charge species, at a minimum singly-charged ions and electrons, instead of only electrons as tracked in typical electrical circuits. Third, the plasma environment contains charge sources, ionization, and charge sinks, recombination, that are time-dependent physical processes and do not provide a closed path for charges as fundamentally required by electrical circuits. To transition the model presented in Figure 3 to an electrical circuit, we must deviate from classical electrical engineering practices and implement a new approach while adhering to charge and energy conservation equations.

VII.Conclusion

Electrical facility effects in EP testing aims to characterize the effects electrically-conductive vacuum chambers have on the performance and stability of HETs. A review of ion-electron recombination physics shows that the energetic plasma exhausted from EP devices require thousands of meters to ensure complete charge neutralization of the plume. Thus, the HET plume will electrically interact with its immediate operational environment to satisfy charge neutrality. A direct comparison between the space and vacuum test facility operational environment shows differences in observed pressures, compositions, and electrical boundary conditions. Given that metallic vacuum chambers are electrically conductive and offer 10^{12} cm^{-3} more free electrons than the space plasma environment, we infer that ion-electron recombination and overall plume neutralization is significantly facilitated by the chamber wall. Thus, for the first time, a theoretical framework has been developed to model the electrical coupling between HET plumes and metallic vacuum test facilities. In doing so, we identified two additional current pathways related to HET plume neutralization present in vacuum test facilities that are absent in space: (1) CEX ion currents neutralizing with side and rear facility surfaces and (2) beam ions neutralizing with downstream facility surfaces. Where appropriate, we derived effective resistances, capacitances, and inductances to capture the physical interaction between the emitted HET plume and the facility. The current pathways model presented is a step forward in understanding and quantifying the impedance of the overall HET discharge as the plume couples to its local operational environment.

Acknowledgments

The authors would like to thank Dr. Dan Lev for many helpful discussions throughout the development of this model. In addition, we would like to thank HPEPL graduate students Janice Cabrera and Chhavi for their support in collecting experimental test data that helped develop the current pathways model and their help in generating the figures presented in this manuscript.

REFERENCES

[1] Grossman, E. and Gouzman, I., "Space Environment Effects on Polymers in Low Earth Orbit," *Nuclear Instruments and Methods in Physics Research Section B: Beam Interactions with Materials and Atoms*, Vol. 208, 2003, pp. 48-57. https://doi.org/10.1016/S0168-583X(03)00640-2

[2] Estublier, D. L., "The SMART-1 Spacecraft Potential Investigations," *IEEE Transactions on Plasma Science*, Vol. 36, No. 5, 2008, pp. 2262-2270. https://doi.org/10.1109/TPS.2008.2002032

[3] Walker, J. A., Langendorf, S. J., Walker, M. L. R., Khayms, V., King, D. and Peterson, P., "Electrical Facility Effects on Hall Current Thrusters: Electron Termination Pathway Manipulation," *Journal of Propulsion and Power*, Vol. 32, No. 6, 2016, pp. 1365 - 1377. https://doi.org/10.2514/1.B35904

[4] Frieman, J. D., Walker, J. A., Walker, M. L. R., Khayms, V. and King, D. Q., "Electrical Facility Effects on Hall Thruster Cathode Coupling: Performance and Plume Properties," *Journal of Propulsion and Power*, Vol. 32, No. 1, 2016, pp. 251 - 264. https://doi.org/10.2514/1.B35683

[5] Peterson, P. Y., Kamhawi, H., Huang, W., Yim, J., Herman, D., Williams, G., Gilland, J. and Hofer, R., "NASA HERMeS Hall Thruster Electrical Configuration Characterization," *52nd AIAA/SAE/ASEE Joint Propulsion Conference*, Salt Lake City, UT, AIAA Paper 2016-5027, July 25 - 27, 2016. https://doi.org/10.2514/6.2016-5027

[6] Hahn, Y., "Electron-Ion Recombination Processes - An Overview," *Reports on Progress in Physics*, Vol. 60, No. 7, 1997, pp. 691-759. https://doi.org/10.1088/0034-4885/60/7/001

[7] Zerrad, E. and Hahn, Y., "Radiative Recombination at Low Energies," *Journal of Quantitative Spectroscopy and Radiative Transfer*, Vol. 59, No. 6, 1998, pp. 637-651. https://doi.org/10.1016/S0022-4073(97)00147-7

[8] Kim, Y. S. and Pratt, R. H., "Direct Radiative Recombination of Electrons with Atomic Ions: Cross Sections and Rate Coefficients," *Physical Review A*, Vol. 27, No. 6, 1983, pp. 2913-2924. https://doi.org/10.1103/PhysRevA.27.2913

[9] Ansari, S. M. R., Elwert, G. and Mücklich, P., "On Dielectronic Recombination," *Zeitschrift für Naturforschung A*, Vol. 25, 1970, pp. 1781-1797. https://doi.org/10.1515/zna-1970-1203

[10] Hahn, Y., "Theory of Dielectronic Recombination," *Advances in Atomic and Molecular Physics*, Vol. 21, 1985, pp. 123-196. https://doi.org/10.1016/S0065-2199(08)60142-6

[11] Safronova, U. I., Bista, R., Bruch, R. and Ralchenko, Y., "Dielectronic Recombination of the Xe^{8+} Ion and Satellite Lines of the Xe^{7+} Ion," *Journal of Physics B: Atomic, Molecular and Optical Physics*, Vol. 42, No. 1, 2008. https://doi.org/10.1088/0953-4075/42/1/015001

[12] Song, M.-Y. and Kato, T., "Dielectronic Recombination of Xe^{10+} Ions and Satellite Line of Xe^{9+} Ions," National Institute for Fusion Science (NIFS), NIFS-DATA-94, Toki, Japan, October 2005.

[13] Hahn, Y., "Improved Rates for Three-Body Recombination at Low Temperature," *Physics Letters A*, Vol. 264, No. 6, 2000, pp. 465-471. https://doi.org/10.1016/S0375-9601(99)00844-0

[14] Baumjohann, W. and Treumann, R. A., *Basic Space Plasma Physics*, 3rd ed., World Scientific, Singapore, 2022, pp. 5 - 11.

[15] Stubbe, P. and Hagfors, T., "The Earth's Ionosphere: A Wall-less Plasma Laboratory," *Surveys in Geophysics*, Vol. 18, January 1997, pp. 57-127.
https://doi.org/10.1023/A:1006583101811

[16] Oyama, K.-I., Abe, T., Sakaide, Y., Kutiev, I., Okuzawa, T., Choi, T. and Choi, Y., "Electron Temperature Distribution in the Inner Plasmasphere I (Mid and Low Latitudes)," *Advances in Space Research*, Vol. 17, No. 10, 1996, pp. 185-188.
https://doi.org/10.1016/0273-1177(95)00711-M

[17] Laakso, H., Opgenoorth, H., Wygant, J., Escoubet, P., Clemmons, J., Johnson, M., Maynard, N., Mozer, F., Pfaff, R. and Scudder, J., "Electron Density Distribution in the Magnetosphere," *31st ESLAB Symposium*, ESTEC, Noordwijk, The Netherlands, ESA SP-415, September 22-25, 1997.

[18] Roeder, J. L., "Specification of the Plasma Environment at Geosynchronous Orbit in the Energy Range 87 eV to 288 keV," The Aerospace Corporation, SMC-TR-96-9, El Segundo, CA, August 1994.

[19] Garrett, H., "The Geosynchronous Plasma Environment," *28th Aerospace Sciences Meeting*, Reno, NV, AIAA Paper 1990-0889, January 1990.
https://doi.org/10.2514/6.1990-289

[20] Yue, C., Bortnik, J., Li, W., Ma, Q., Gkioulidou, M., Reeves, G. D., Wang, C.-P., Thorne, R. M., Lui, A. T. Y., Gerrard, A. J., Spence, H. E. and Mitchell, D. G., "The Composition of Plasma inside Geostationary Orbit Based on Van Allen Probes Observations," *Journal of Geophysical Research: Space Physics*, Vol. 123, No. 8, 2018, pp. 6478-6493.
https://doi.org/10.1029/2018JA025344

[21] Takeda, M. and Araki, T., "Electric Conductivity of the Ionosphere and Nocturnal Currents," *Journal of Atmospheric and Terrestrial Physics*, Vol. 47, No. 6, 1985, pp. 601-609.
https://doi.org/10.1016/0021-9169(85)90043-1

[22] Piragino, A., Faraji, F., Reza, M., Ferrato, E., Piraino, A. and Andreussi, T., "Background Pressure Effects on the Performance of a 20 kW Magnetically Shielded Hall Thruster Operating in Various Configurations," *Aerospace*, Vol. 8, No. 3, 2021, Article No. 69.
https://doi.org/10.3390/aerospace8030069

[23] Kittel, C., "Free Electron Fermi Gas", *Introduction to Solid State Physics*, 8th ed., Wiley, New Jersey, 2004, pp. 131-159.

[24] Mills, K. C., Su, Y., Li, Z. and Brooks, R. F., "Equations for the Calculation of the Thermo-physical Properties of Stainless Steel," *Transactions of the Iron and Steel Institute of Japan International*, Vol. 44, No. 10, 2004, pp. 1661-1668.
https://doi.org/10.2355/isijinternational.44.1661

[25] Jovel, D. R., Walker, M. L. R. and Herman, D., "Review of High-Power Electrostatic and Electrothermal Electric Propulsion," *Journal of Propulsion and Power*, Vol. 38, No. 6, 2022, pp. 1051-1081.
https://doi.org/10.2514/1.B38594

[26] Yim, J., "A Survey of Xenon Ion Sputter Yield Data and Fits Relevant to Electric Propulsion Spacecraft Integration," *35th International Electric Propulsion Conference*, Atlanta, GA, IEPC Paper 2017-060, October 2017.

[27] Peterson, P., Kamhawi, H., Huang, W., Yim, J. T., Haag, T. W., Mackey, J. A., McVetta, M. S., Sorrelle, L. T., Tomsik, T. M., Gilligan, R. P. and Herman, D. A., "Reconfiguration of NASA GRC's Vacuum Facility 6 for Testing of Advanced Electric Propulsion System (AEPS) Hardware," Vantage Partners, LLC, NASA/TM-2018-219717, Brook Park, OH, February 2018.

[28] Miller, J. S., Pullins, S. H., Levandier, D. J., Chiu, Y.-h. and Dressler, R. A., "Xenon Charge Exchange Cross Sections for Electrostatic Thruster Models," *Journal of Applied Physics*, Vol. 91, No. 3, 2002, pp. 984 - 991.
https://doi.org/10.1063/1.1426246

[29] Chen, F. F., "Time-Varying Impedance of the Sheath on a Probe in an RF Plasma," *Plasma Sources Science and Technology*, Vol. 15, No. 4, 2006, pp. 773 - 782.

https://doi.org/10.1088/0963-0252/15/4/022

[30] Godyak, V. A., Piejak, R. B. and Alexandrovich, B. M., "Electrical Characteristics of Parallel-Plate RF Discharges in Argon," *IEEE Transactions on Plasma Science*, Vol. 19, No. 4, 1991, pp. 660 - 676. https://doi.org/10.1109/27.90309

[31] Choueir, E. Y., "Plasma Oscillations in Hall Thrusters," *Physics of Plasmas*, Vol. 8, No. 4, 2001, pp. 1411 - 1426. https://doi.org/10.1063/1.1354644